Carbon Nanotubes: How Strong Is Their Bond with the Substrate?

Indranil Lahiri,[†,⊥] Debrupa Lahiri,[‡,⊥] Sungho Jin,[§] Arvind Agarwal,[‡,*] and Wonbong Choi[†,*]

[†]Nanomaterials and Device Laboratory, and [‡]Nanomechanics and Nanotribology Laboratory, Department of Mechanical and Materials Engineering, Florida International University, Miami, Florida 33174, United States, and [§]Department of Mechanical and Aerospace Engineering, University of California, San Diego, La Jolla, California 92093, United States. [⊥] These authors contributed equally in this work.

ABSTRACT A reliable quantification technique for interpreting nanomaterial−substrate bond strength is highly desired to predict efficient, long-term performance of nanomaterial-based devices. Adopting a novel nanoscratch-based technique, here we demonstrate quantification of carbon nanotube (CNT)−substrate adhesion strength for dense CNT structure and for patterned carbon nanocone (CNC) structures. Debonding energy for a single CNT is illustrated to range between 1 and 10 pJ, and the variation is strongly dependent on the nature of the interface between CNTs, catalysts, and substrates. Our proposed technique could be adopted for characterization of bonding strength between a wide variety of nanotubes, nanowires, and other one-dimensional nanostructured materials and their underlying substrates.

KEYWORDS: nanotubes · adhesion · nanoscratch · bonding energy

A wide variety of one-dimensional nanomaterials, such as nanotubes and nanowires, are proposed for improved performance of a number of future devices—from sensors to solar cells.[1,2] However, desired seamless integration, long-time, reliable performance, and extended device lifetime of all these nanomaterials-based devices necessitates stability of the structure.[3−5] One of the critical issues in structural stability is the bonding between the nanomaterials and the substrate. A poor nanomaterial−substrate adhesion may cause unreliable behavior and a very short life span of such a device. Hence, knowledge about nature and strength of the nanostructure−substrate bond is considered as one of the most fundamental issues. It is of utmost importance to devise a methodology to quantify the nanomaterial−substrate bonding, to apply that technique to understand bonding between different nanostructure−substrate bonding, ultimately leading to development of well-bonded nanostructured devices.

Among all the one-dimensional (1-D) nanomaterials, carbon nanotubes (CNT) are probably the most important for a myriad of potential next generation devices, owing to their fascinating properties, such as unique structures,[6] excellent electronic and electrical properties,[7,8] high specific strength,[9] good thermal conductivity,[10] and chemical inertness.[11] Almost two decades of intense research activities have resulted in the demonstration of various CNT-based devices, for example, nanoelectronics, field emission displays,[12,13] biosensors and biomaterials,[14,15] and hydrogen storage and energy generation devices.[16−18] Research efforts (Supporting Information Table S1) to clarify the nature of bonding between nanomaterials and substrates are thus mostly restricted to CNT-based systems. However, the qualitative methods utilized do not offer any standardized procedure and reproducible results, as the techniques are extremely user sensitive. The quantitative methods experimented so far have some common ground for comparison of adhesion strengths, though all of these techniques pose several limitations. First, none of these methods have been calibrated to single out the bonding between only CNT−substrate. Proposed quantitative methods do not show the amount of stress required to pull out the adhesive tape from a blank substrate (without having CNTs grown on it).[3,4,19] Thus, the strength values found in these methods are often overestimated values of exact contribution from the CNT−substrate bond. Second, the adhesion strength was calculated assuming the area of the tape as the contact area. The actual contact area, where CNTs are in contact with the tape, is much lower. So, the reported values are likely to be an underestimate of the actual strength required to debond CNTs from the substrate. Third, the number of CNTs in contact with the tape was not known, and hence, none of these methods could predict adhesion strength of a single CNT. Furthermore, it was not known whether the CNTs were breaking at the CNT−substrate interface or at any defective locations along its length or if one or few

*Address correspondence to choiw@fiu.edu, agarwala@fiu.edu.

Received for review June 18, 2010 and accepted December 20, 2010.

Published online January 05, 2011
10.1021/nn102900z

layers of multiwall CNTs were being detached or whether the CNTs were detaching from the adhesive tape itself and not removed from the substrate. These uncertainties of the reported methods lead to unknown errors in the evaluation of bond strength. Therefore, it is essential to design a new test methodology, which can more reliably characterize the bond strength between 1-D nanomaterials and their substrates.

In the present study, we developed a new methodology of nanoscratch technique to quantify nanomaterial−substrate bonding, overcoming the limitations of existing techniques. CNTs, being the most popular material among 1-D nanomaterials, are selected as the experimental material for this study. Since the area of importance for CNT−substrate adhesion is their interface, we aimed to apply a nanolevel characterization technique to the interface and developed a nanoscratch-based method to quantify CNT−substrate bonding energy. Nanoscratch technique is well-established for measurement of mechanical properties in two-dimensional nanomaterials, such as thin films used in magnetic storage materials, microelectromechanical systems (MEMS), *etc.*[20,21] To the best of our knowledge, this is the first study to apply nanoscratch technique to 1-D nanomaterials systems, for quantifying their adhesion with the substrates.

RESULTS AND DISCUSSION

The nanoscratch-based technique was applied to quantify bonding energy of CNTs on two different types of substrates, Cu and Si, both having Ti and Ni as barrier layer and catalyst, respectively (see Materials and Methods section). Though CNTs can be synthesized on a wide variety of substrates,[4,22] our choice of Cu substrate is inspired by our recent studies, in which randomly oriented multiwall CNT structure, directly grown on Cu substrate, has shown excellent properties for application in Li-ion battery electrodes and field emission devices, which was attributed to the stable interfacial structure.[18,23] On the other hand, Si has been the most widely used substrate material for CNT-based devices.[5] Details about both the substrate materials are given in Materials and Methods section.

On both the Cu and Si samples, dense, randomly oriented CNTs were grown by thermal chemical vapor deposition (CVD) (30 min growth time) (Figure 1a,b). To understand the nature of the samples, SEM and Raman spectroscopy were performed for both the samples. Raman spectra (Figure 1c) taken from these samples show broadening of D and G peaks, shift of the G peak (toward higher frequency), and a high ($\geq$1.0) peak intensity ratio (I_D/I_G). It may be recalled here that first-order Raman spectra of all graphitic materials, including CNTs, show a "G" band at 1580 cm^{-1} (which is high-frequency E_{2g} first-order mode from graphite-like

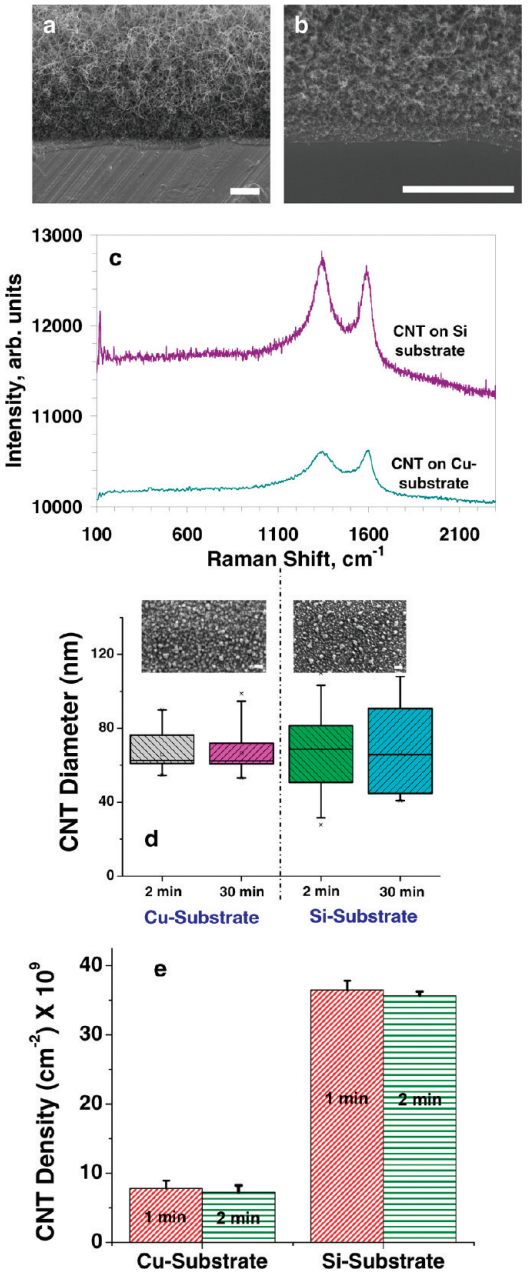

Figure 1. Structural features of CNTs on Cu and Si substrates. (a,b) SEM images of CNTs on Cu and Si substrates (scale bar length is 10 μm), respectively. (c) Comparison of Raman spectra of the CNTs grown on both Cu and Si substrates. (d) Plot of diameter distribution of CNTs on both substrates, at two different growth times, 2 and 30 min. Insets show SEM images of catalytic islands on both samples, and the images were taken just before CNT growth (scale bar length is 200 nm). (e) Density of CNTs for both the samples, after 1 and 2 min of CVD growth.

sp^2-type bonds), along with a "D" band at 1350 cm^{-1} (which is originated from diamond-like sp^3 bonds).[24] Since the origin of the D band can be explained by double resonance theory, it is also indicated as A_{1g} D mode—a band caused by defects and disorder of the graphitic material. In the present study, comparatively wider peaks of D and G bands indicate presence of disorder-induced features in the graphite-like (sp^2)

material and predominance of tubular structures in the CNTs, respectively. Moreover, a high ratio of I_D/I_G peaks ($\geq$1.0) shows that the multiwalled CNT structure has high defect density.[25] Thermal CVD process is known to produce randomly oriented, thicker CNTs.[26] Vertical alignment of CNTs is possible in a plasma-enhanced CVD (PECVD) process or on materials such as porous Si, anodic aluminum oxide (AAO), and prepatterned substrates. CVD-grown CNTs are conventionally found to have less crystalline structure, that is, higher fraction of defects and larger diameters, as compared to CNTs synthesized through an arc−discharge method.[27] Hence, CNT structure observed in the present study is in agreement with the expected structure.

Figure 1d presents a quantitative estimation of the diameters of CNTs on both substrates as a function of growth time. It can be seen that the diameter of CNTs is almost independent of growth time, irrespective of substrates, although CNTs on the Si substrate showed much wider diameter distribution. This fact is also supported by the observation reported by Bedewy *et al.*, who have noted a maximum of 5−10% change in CNT diameter during the growth period.[28] Moreover, in line with the *in situ* observation of CNT nucleation by Hofmann *et al.*,[29] we also observed that CNT nucleation was almost instantaneous and only the growth in the longitudinal direction predominates with growth time. Though during growth process, some CNTs may terminate or debond from the substrate abruptly,[28,30] CNT density was not found to change much with growth time. To gain further insight into this aspect, CNT densities were measured for both types of samples, after 1 and 2 min of growth time (Figure 1e). CNT density was found to remain nearly constant with growth time, although it was higher for the Si substrate, as compared to the Cu substrate. This difference in density of CNTs on Cu and Si substrates may be correlated with the distribution of catalytic nanoislands on these two surfaces (insets of Figure 1d). It is well-known that the catalytic island formation initiates by dewetting from the substrate surface, and final shape, size, and crystallinity of these islands depend strongly on the minimization of surface and interface energy.[31] Initial thickness of the catalyst film also plays an important role.[32] Another important factor to explain variation in catalytic island number and size distribution may be differential solubility of catalytic layers in Cu and Si substrates. Higher solubility of Ti in Cu (1 wt %, as compared to 0 solubility of Ti in Si,[33] at growth temperature) leads to an onset of interdiffusion and imposes additional constraints for breakage of the thin film, resulting in a formation of less number of nanoislands. However, in the absence of any such factors for Si (due to almost 0 solubility of the catalyst in Si[33]), catalytic island formation is solely governed by wetting, presence of surface defects, *etc.* and leads to a wider distribution. After clarifying all of the structural issues, like diameter, length, and density of CNTs on these two different substrates, we concentrated our focus on quantifying the bonding between CNT−substrates through nanoscratch tests.

Nanoscratches, using a standard Berkovich indenter (with 100 nm tip radius), were made in such a way that each scratch started from a bare surface and then traversed through the CNT forest, using a constant normal load (see Materials and Methods and Supporting Information Figure S1). While moving through the CNTs, the indenter tip faces an extra opposing force, which is reflected through an increased lateral force on the tip. To calibrate the samples with respect to the contributions of substrates and the catalyst thin films on the lateral force behavior, comparative nanoscratch tests were conducted on bare substrates, substrates after thin catalyst film deposition, and finally, after CNT growth. Responses from these three types of samples were found to be clearly different (Supporting Information Figure S2). Figure 2a (for Cu substrate) and Figure 2b (for Si substrate) show that, in the presence of CNTs, the indenter tip experiences a much higher lateral force. Figure 2c,d (and their insets) shows the nanoscratch images from Cu and Si samples, respectively (after CNT growth), indicating that CNTs were removed from the area of the scratches. Increased lateral forces for both samples are actually responsible for breaking the CNT−substrate bonds and uprooting the CNTs from the respective substrates. One important observation to be made from Figure 2a,b is the effect of the Ti underlayer. Inability of Si and Ti to form a solid solution[33] leads to retention of Ti as a separate layer (which is clearly visible as a separate layer in the SPM images presented in Supporting Information Figure S3), which exerts an extra opposing force on the indenter. This force appears as a peak in the lateral force curve for the Si substrate (Figure 2b). However, in the case of the Cu substrate, good solid solubility of Ti in Cu leads to extensive interdiffusion and, thus, disappearance of any separate layer on Cu substrate (see Supporting Information Figure S3).

One more important issue to be noticed is the effect of initial surface roughness of the substrates. Cu−substrate had a rougher surface compared to the Si wafer. This was reflected in the nanoscratch plots also (Figure 2a,b)—scratching through the bare Cu substrate shows much more lateral force compared to the Si substrate. Thus, the nanoscratch technique is able to distinguish effects from substrate, catalyst, and CNTs. Increments in the lateral force, which can be interpreted as adhesion or bonding force of CNTs with their substrates, are plotted in Figure 2e, for five scratches per sample and for two different growth times of 2 and 30 min (Supporting Information Figure S4). It may be observed that growth time does not affect the lateral force in any significant way for both Cu and Si substrates. As higher growth time is related to longer CNTs,

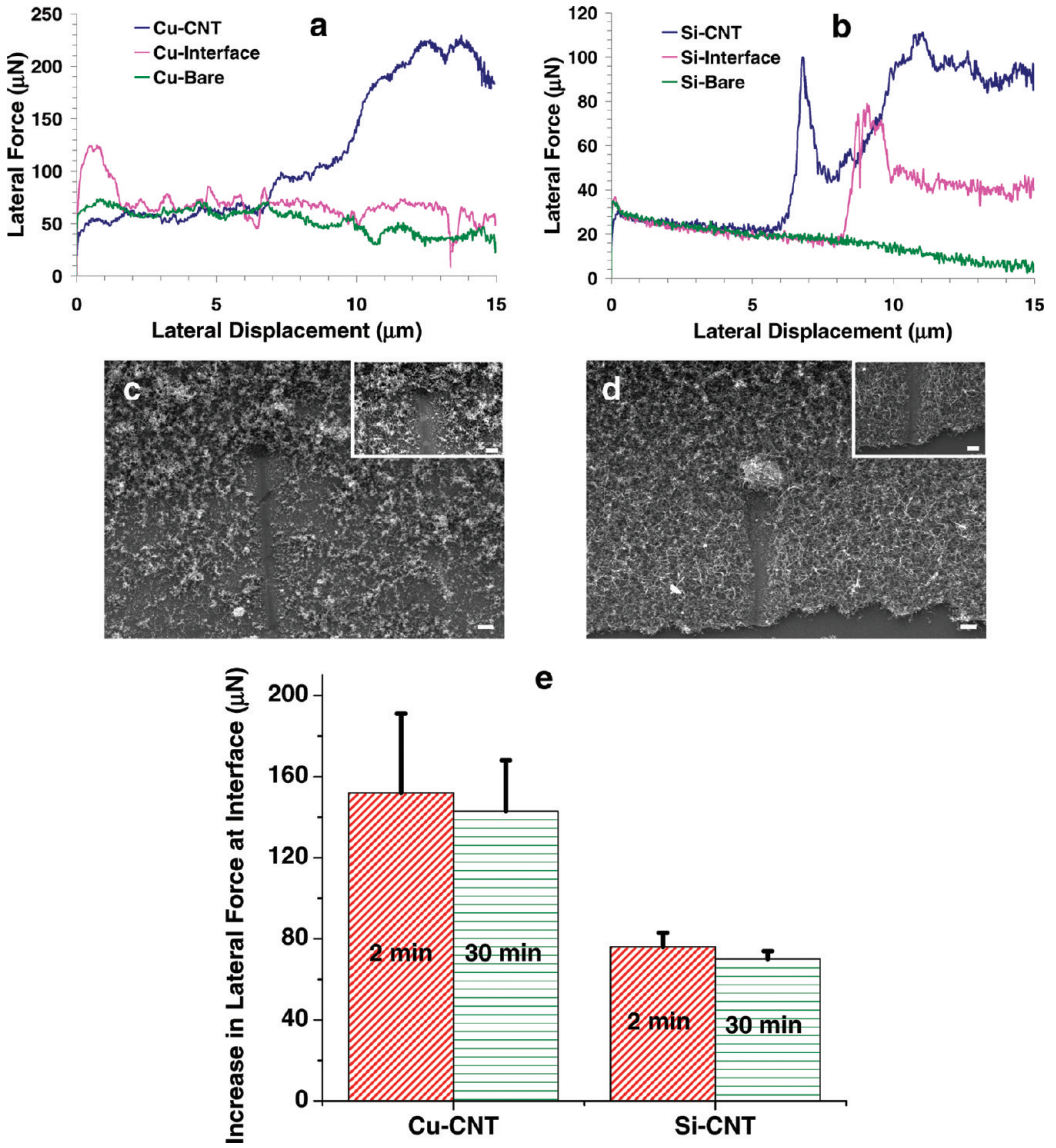

Figure 2. Nanoscratch through CNTs on different substrates. Lateral force response during nanoscratch tests on (a) Cu−CNT and (b) Si−CNT samples. Curves represent force required to scratch bare substrates, substrates with only catalysts and substrates after CNT growth. (c,d) SEM images of nanoscratches through the CNT structure on Cu and Si substrates, respectively. Insets show higher magnification SEM images of the scratches (scale bar length is 1 μm). (e) Plot of lateral force increment for both Cu−CNT and Si−CNT samples, after 2 and 30 min of growth time.

it seems that long CNTs, which form a dense, tangled network, do not exert any extra load on the indenter. Hence, the increment in lateral force is mainly due to uprooting of CNTs from their substrates. Figure 2e also points out that the force required to debond CNTs from the Cu substrate is much higher (almost 2 times) as compared to that of the Si substrate. Thus, CNTs can be removed from the Si substrate with a much lower force than that required to detach CNTs from the Cu substrate. During CVD growth, the Ti underlayer reacts with carbon precursor gas and forms TiC, providing a strong bonding between the underlayer and the CNTs.[23] However, to achieve better adhesion of CNTs to the substrate, it is necessary that the substrate and the underlayer form a strong bond. Comparison of Cu−Ti and Si−Ti phase diagrams indicates that solid solubility of Ti in Cu may promote formation of such bond between Cu and Ti, while nil solubility of Ti in Si may prevent formation of any such bond.[33] However, interfaces need to be studied in detail for a better understanding of this issue.

After quantifying the forces required to debond a dense forest of CNTs from Cu and Si substrates, we made an effort to illustrate the bonding energy of an individual CNT with the substrates. For this calculation, average densities of CNTs were taken for all samples. Due to extensive entanglement, CNTs could not be counted for samples having a growth time more than 2 min during the present study. It was observed that until 2 min growth time, CNT density remained almost

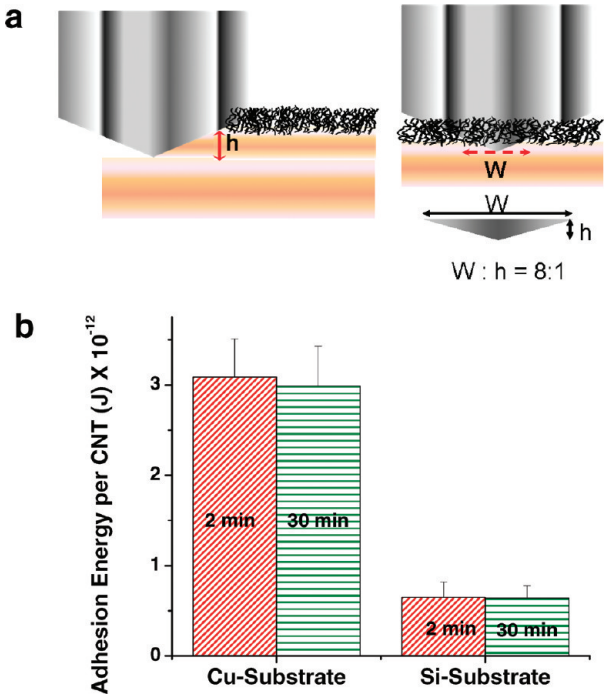

Figure 3. Calculation of adhesion energy of single CNT. (a) Schematic of the nanoscratch technique, emphasizing on the geometry of the Berkovich indenter. (b) Comparison of adhesion energy of individual CNTs on both Cu and Si substrates.

constant (Figure 1e).[28] Therefore, it was assumed that CNT density remained constant throughout the growth period. Though self-termination (sudden and sharp fall in growth rate) is reported to be observed during CNT growth,[28] which may decrease CNT density, it was found to occur at higher temperatures (>1283 K).[30] Moreover, time to initiate "self-termination" was strongly dependent on growth temperature and found to increase sharply with lower growth temperature. During the present study, CNT growth was performed at a much lower temperature of 973K. Following the trend reported in ref 30, it is expected that the effect of self-termination on CNT density would be minimum during the present study. However, nanoscratch tests were performed on 2 min CNT growth samples also, for which CNT density was calculated (in addition to 30 min CNT growth samples), and results from both types of samples were compared.

Figure 3a shows a schematic of geometry of the tip and the parameters required for the bond energy calculation. The indentation depth, *h*, was available for each scratch, in the normal displacement plots generated by the software. Figure 3b presents the bond energy of individual CNTs on different substrates. As the diameter of CNTs remains almost constant but length increases with growth time, the difference in bonding energy of 2 *versus* 30 min growth samples could be related to the effect of CNT length. This difference was found to show a variation of 1−2% for both Cu and Si substrates, while the actual calculated debonding energy values range over ±15% of the mean. Hence, the CNT length effect on the debonding energy is considered to be negligible. The energy calculated thus represents the energy required to debond a single CNT. It may be observed that ∼3 pJ energy is required to debond one single CNT from the Cu−substrate, which is equivalent to breaking 5 million C−C bonds.[34] It may be noted here that the adhesion energy for CNTs from Cu−substrate is ∼4.7 times higher than that of Si−substrate, while the debonding force was nearly 2 times higher for CNTs on Cu−substrate than that on Si−substrate. The difference in the factor is due to CNT density difference among both samples. It will be appropriate to mention here that the bonding energy of single CNTs, as calculated above, is true only for the materials and methods used in the present study and may vary depending on the experimental conditions followed. Different processing conditions are known to synthesize different varieties of CNTs.[35] Detailed understanding of all such factors on bonding energy of the CNT−substrate may be addressed in a future study. The present study aimed to show feasibility of the nanoscratch technique to quantify nanotube−substrate bonding up to a single nanotube level.

In order to show its ability to directly quantify adhesion energy down to single nanostructure level, we considered an explicitly different 1-D nanostructure—a periodically spaced and vertically aligned carbon nanocone (CNC) structure grown on a lithographically prepatterned Si substrate.[36] Figure 4a,b

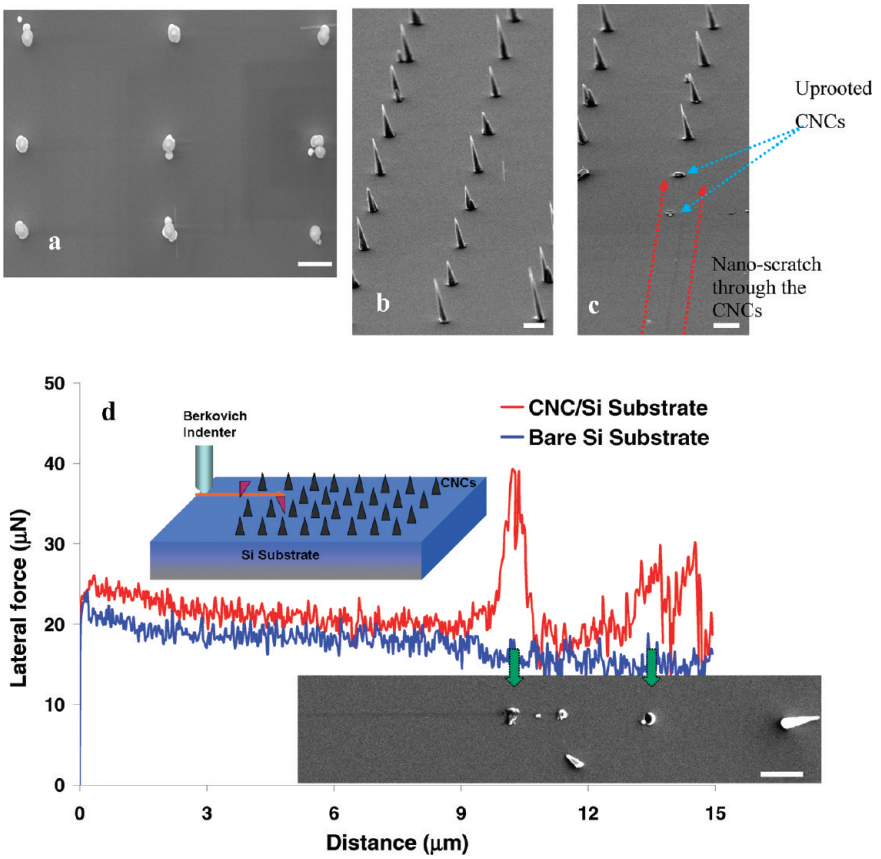

Figure 4. Nanoscratch on nanopatterned carbon nanocone structure. (a−c) SEM images of the CNC structure: (a) before nanoscratch, imaged at a tilt angle of ∼40°; (b) before nanoscratch, imaged from top, showing the presence of multiple CNCs in each catalytic islands; and (c) after nanoscratch showing removal of CNCs, imaged at a tilt angle of ∼40°. (d) Lateral force response during nanoscratch test on the Si−CNC sample, comparing effects on bare substrate and through CNCs. The top inset shows a schematic of the process, uprooted CNCs being shown in a different color. The lower inset shows the corresponding SEM image. All scale bars in this figure are 1 μm.

shows typical SEM images of the structure, where each catalyst island is observed to accommodate 1−3 CNCs. Each island is ∼300 nm in diameter, and the CNCs formed on these islands are ∼2 μm in length. Nanoscratches made on this sample clearly show uprooting of individual CNCs, both in SEM images and in corresponding quantitative data (Figure 4c,d and the lower inset of panel d). Appearance of peaks in the nanoscratch plot (Figure 4d) could easily be correlated with the distance between consecutive nanocone islands. Separate peaks for each island of nanocones show high resolution of the nanoscratch technique to quantify debonding force for a single nanocone structure. Force required to debond CNCs in each island is found to vary between 10 and 25 μN, depending on the number of CNCs present in each island. This corresponds to a debonding energy of 8−10 pJ per CNC. However, it may be noted here that the debonding energy for CNCs includes the effect of catalysts. Synthesis techniques and parameters used for CNCs and CNTs (as mentioned earlier) are totally different. Furthermore, CNCs have a much higher contact area (having a solid base diameter of ∼300 nm) than the CNTs (ring-type base, with a diameter in the range of 60−80 nm). As mentioned before, the CNT−substrate bond is a strong function of the properties of materials, synthesis conditions, and their exact contact area. Thus, debonding energy values, as measured for the CNCs and CNTs, are not directly comparable. However, the nanoscratch test on CNC sample shows its direct application in single nanotube/nanowire samples, too.

Summarizing, in the present study, a nanoscratch-based technique was successfully utilized to quantify nanotube−substrate adhesion strength down to an individual nanotube level on different substrates. The technique efficiently overcomes most of the limitations encountered in previously reported studies by providing calibration against the effect of substrate materials and catalyst layers and avoiding overestimation of contact area. The SEM images after nanoscratching prove that the CNTs were definitely up-rooted from the substrate. The nanoscratch technique also enables us to directly quantify debonding energy of individual CNCs. This novel method is simplistic in nature, independent of operators' skill, fully reproducible, and can be calibrated for the contributions from substrate and catalysts. In the future,

this technique is anticipated to be adopted for characterization of bonding between substrate and any kind of 1-D nanostructure (nanotube, nanowire, nanofiber, nanocones, *etc.*) grown on a given substrate.

MATERIALS AND METHODS

Pure (99.95%) Cu sheets and Si wafers were chosen as the substrates for CNT growth. The Cu and Si samples had an average surface roughness value of 12.43 ± 1.25 nm (rms roughness value 15.83 ± 1.60 nm) and 5.25 ± 0.06 nm (rms roughness value 6.33 ± 0.11 nm), respectively. CNTs were grown directly on these substrates using a thermal chemical vapor deposition (CVD) method, predeposited with thin (~20 nm) sputtered films of Ti (as underlayer) and Ni (as catalyst). Ti and Ni were deposited on the substrates using a radio frequency (RF) magnetron sputtering system (AJA International). Scanning probe microscopic (SPM) images of both types of samples, before and after catalyst deposition, can be found in Supporting Information Figure S3. CVD was carried out at temperatures and time of 973 K and 1−30 min, respectively, and under $H_2 + C_2H_4$ gas mixture (in 1:2 ratio). During the initial stage of CVD, samples were heated very fast under an Ar gas envelope. Samples were slowly cooled to room temperature in an Ar gas envelope within the furnace, after completion of CNT growth.

Nanoscratch tests were done on these samples in a Hysitron Triboindenter, using a normal load of 150 μN. Length of each scratch was kept constant at 15 μm (see Figure S1 in Supporting Information for a schematic of the scratch test). Analysis of the scanning probe microscopy (SPM) images was performed by SPIP software. Structural characterization of the samples, before and after nanoscratch tests, was performed in JEOL JSM7000F field emission scanning electron microscope and Raman spectrometer (Ar^+ laser with λ = 514 nm, 15 mW power).

Before synthesis of carbon nanocones (CNCs), Ni catalyst was deposited on Si substrate using electron beam lithography process. CNCs were grown on these catalyst islands in a direct current plasma-enhanced chemical vapor deposition (DC-PECVD) system. Morphology of the CNCs was controlled through adjustment of DC bias during growth. Details about the CNC synthesis is available in ref 36.

For calculation of debonding energy, the following relations were used.

$$\begin{aligned} A &= W \times L \\ W &= 8 \times h \\ E &= F \times L \\ N &= \rho \times A \\ E^0 &= E / N \end{aligned}$$

where A = area of interest, μm^2; W = width of scratch, μm; L = arbitrary length of scratch, taken as 1 μm; h = normal displacement as measured from the normal displacement plots generated by the software, nm; E = energy to debond CNTs, pJ; F = lateral force as measured from lateral force−displacement plots generated by the software, μN; N = number of CNTs in area of interest, A; ρ = CNT density (as measured from SEM images), per μm^2; E^0 = energy required to debond each CNT, pJ per CNT.

Lateral force values (F) used in this calculation were calibrated to subtract the effects of substrates and catalysts.

During CNT diameter and density calculations, 50 images (which is a statistically significant number) were captured at high magnification (>30 000×) for each type of sample. The diameter of each of the CNTs present in those images and the number of CNTs in the area of images were counted on each of these images using ImageJ software.[37] For CNT density calculation, the counted number for CNTs for each image was divided by the area of the image.

Acknowledgment. I.L. and W.C. acknowledge financial support from NSF Grant NSF CMMI-0900583 and AFOSR Grant FA9550-09-1-0544. I.L. further acknowledges Dissertation Evidence Acquisition Fellowship from University Graduate School, Florida International University. A.A. would like to acknowledge support from National Science Foundation CAREER Award (NSF-DMI-0547178) and ONR-DURIP (N00014-06-0675) grant. D.L. thanks FIU University Graduate School for awarding Dissertation Evidence Acquisition Fellowship.

Supporting Information Available: Comparison table for CNT−substrate adhesion testing methods, schematic of the test method, SPM images of substrates and nanoscratches, and extra plots of nanoscratch tests. This material is available free of charge *via* the Internet at http://pubs.acs.org.

REFERENCES AND NOTES

1. Wang, X.; Ozkan, C. S. Multisegment Nanowire Sensors for the Detection of DNA Molecules. *Nano Lett.* **2008,** *8*, 398–404.
2. Sivakov, V.; Andrä, G.; Gawlik, A.; Berger, A.; Plentz, J.; Falk, F.; Christiansen, S. H. Silicon Nanowire-Based Solar Cells on Glass: Synthesis, Optical Properties, and Cell Parameters. *Nano Lett.* **2009,** *9*, 1549–1554.
3. Cao, A.; Veedu, V. P.; Li, X.; Yao, Z.; Ghasemi-Nejhad, M. N.; Ajayan, P. M. Multifunctional Brushes Made from Carbon Nanotubes. *Nat. Mater.* **2005,** *4*, 540–545.
4. Talapatra, S.; Kar, S.; Pal, S. K.; Vajtai, R.; Ci, L.; Vicor, P.; Shaijumon, M. M.; Kaur, S.; Nalamasu, O.; Ajayan, P. M. Direct Growth of Aligned Carbon Nanotubes on Bulk Metals. *Nat. Nanotechnol.* **2006,** *1*, 112–116.
5. Su, H.-C.; Chen, C.-H.; Chen, Y.-C.; Yao, D.-J.; Chen, H.; Chang, Y.-C.; Ywe, T.-R. Improving the Adhesion of Carbon Nanotubes to a Substrate Using Microwave Treatment. *Carbon* **2010,** *48*, 805–812.
6. Saito, R.; Dresselhaus, G.; Dresselhaus, M. S. *Physical Properties of Carbon Nanotubes*; Imperial College Press: London, 1998; pp 35−58.
7. Durkop, T.; Getty, S. A.; Cobas, E.; Fuhrer, M. S. Extraordinary Mobility in Semiconducting Carbon Nanotubes. *Nano Lett.* **2004,** *4*, 35–39.
8. Yao, Z.; Kane, C. L.; Dekker, C. High-Field Electrical Transport in Single-Wall Carbon Nanotubes. *Phys. Rev. Lett.* **2000,** *84*, 2941–2944.
9. Dresselhaus, M. S.; Dresselhaus, G.; Eklund, P. C. *Science of Fullerenes and Carbon Nanotubes*; Academic Press: New York, 1996; pp 765−802.
10. Hone, J.; Whitney, M.; Zettl, A. Thermal Conductivity of Single Walled Carbon Nanotubes. *Syn. Metals* **1999,** *103*, 2498–2499.
11. Bonard, J.-M.; Salvetat, J.-P.; Stöckli, T.; de Heer, W. A.; Forró, L.; Châtelain, A. Field Emission from Single-Wall Carbon Nanotube Films. *Appl. Phys. Lett.* **1998,** *73*, 918–920.
12. Choi, W. B.; Chung., D. S.; Kang, J. H.; Kim, H. Y.; Jin, Y. W.; Han, I. T.; Lee, Y. H.; Jung, J. E.; Lee, N. S.; Park, G. S.; *et al.* Fully Sealed High-Brightness Carbon Nanotube Field Emission Display. *Appl. Phys. Lett.* **1999,** *75*, 3129–3131.
13. Wang, Q. H.; Setlur, A. A.; Lauerhaas, J. M.; Dai, J. Y.; Seelig, E. W.; Chang, R. P. H. A Nanotube-Based Field-Emission Flat Panel Display. *Appl. Phys. Lett.* **1998,** *72*, 2912–2913.
14. Besteman, K.; Lee, J. O.; Wiertz, F. G. M.; Heering, H. A.; Dekker, C. Enzyme-Coated Carbon Nanotubes as Single-Molecule Biosensors. *Nano Lett.* **2003,** *3*, 727–730.
15. Harrison, B. S.; Atala, A. Carbon Nanotube Applications for Tissue Engineering. *Biomaterials* **2007,** *28*, 344–353.
16. Sgobba, V.; Guldi, D. M. Carbon Nanotubes—Electronic/Electrochemical Properties and Application for Nanoelectronics and Photonics. *Chem. Soc. Rev.* **2009,** *38*, 165–184.
17. Liu, C.; Cheng, H. M. Carbon Nanotubes for Clean Energy Applications. *J. Phys. D: Appl. Phys.* **2005,** *38*, R231.

18. Lahiri, I.; Oh, S.-W.; Hwang, J.-Y.; Cho, S.; Sun, Y.-K.; Banerjee, R.; Choi, W. High Capacity and Excellent Stability of Lithium Ion Battery Anode Using Interface-Controlled Binder-Free Multiwall Carbon Nanotubes Grown on Copper. *ACS Nano* **2010,** *4*, 3440–3446.
19. Zhang, Y.; Suhir, E.; Xu, Y.; Gu, C. Bonding Strength of a Carbon Nanofiber Array to Its Substrate. *J. Mater. Res.* **2006,** *21*, 2922–2926.
20. Lee, K. M.; Polycarpou, A. A. Shear Strength Determination Using the Nanoscratch Technique and Its Application to Thin Solid Films. *J. Mater. Res.* **2006,** *21*, 2304–2313.
21. Li, X.; Bhushan, B. A Review of Nanoindentation Continuous Stiffness Measurement Technique and Its Applications. *Mater. Charact.* **2002,** *48*, 11–36.
22. Nessim, G. D.; Seita, M.; O'Brien, K. P.; Mitchell, R. R.; Hart, A. J.; Thompson, C. V. Low Temperature Synthesis of Vertically Aligned Carbon Nanotubes with Ohmic Contact to Metallic Substrates Enabled by Thermal Decomposition of the Carbon Feedstock. *Nano Lett.* **2009,** *9*, 3398–3405.
23. Lahiri, I.; Seelaboyina, R.; Hwang, J. Y.; Banerjee, R.; Choi, W. Enhanced Field Emission from Multi-Walled Carbon Nanotubes Grown on Pure Copper Substrate. *Carbon* **2010,** *48*, 1531–1538.
24. Antunes, E. F.; Lobo, A. O.; Corat, E. J.; Trava-Airoldi, V. J.; Martin, A. A.; Verssimo, C. Comparative Study of First- and Second-Order Raman Spectra of MWCNT at Visible and Infrared Laser Excitation. *Carbon* **2006,** *44*, 2202–2211.
25. Wang, L.; Wang, X.; Wang, L.; Zhang, L. Field Emission Characteristics of Nano-Structured Carbon Films Deposited on Differently Pretreated Mo Films. *Appl. Surf. Sci.* **2008,** *255*, 3257–3262.
26. Ikuno, T.; Honda, S. I.; Furuta, H.; Aoki, K.; Hirao, T.; Oura, K.; Katayama, M. Correlation between Field Electron Emission and Structural Properties in Randomly and Vertically Oriented Carbon Nanotube Films. *Jpn. J. Appl. Phys.* **2005,** *44*, 1655–1660.
27. Bonard, J. M.; Kind, H.; Stöckli, T.; Nilsson, L. O. Field Emission from Carbon Nanotubes: The First Five Years. *Solid-State Electron.* **2001,** *45*, 893–914.
28. Bedewy, M.; Meshoy, E. R.; Guo, H.; Verploegen, E. A.; Lu, W.; Hart, A. J. Collective Mechanism of Evolution and Self-Termination of Vertically Aligned Carbon Nanotube Growth. *J. Phys. Chem. C* **2009,** *113*, 20576–20582.
29. Hofmann, S.; Sharma, R.; Ducati, C.; Du, G.; Mattevi, C.; Cepek, C.; Cantoro, M.; Pisana, S.; Parvez, A.; Cervantes-Sodi, F.; *et al. In Situ* Observations of Catalyst Dynamics during Surface-Bound Carbon Nanotube Nucleation. *Nano Lett.* **2007,** *7*, 602–608.
30. Meshot, E. R.; Hart, A. J. Abrupt Self-Termination of Vertically-Aligned Carbon Nanotube Growth. *Appl. Phys. Lett.* **2008,** *92*, 113107.
31. Hansen, P. L.; Wagner, J. B.; Helveg, S.; Rostrup-Nielson, J. R.; Clausen, B. S.; Topsoe, H. Atom-Resolved Imaging of Dynamic Shape Changes in Supported Copper Nanocrystals. *Science* **2002,** *295*, 2053–2055.
32. Pisana, S.; Cantoro, M.; Parvex, A.; Holfmann, S.; Ferrari, A. C.; Robertson, J. The Role of Precursor Gases on the Surface Restructuring of Catalyst Films during Carbon Nanotube Growth. *Phys. E* **2007,** *37*, 1–5.
33. *Metals Handbook: Metallography, Structures and Phase Diagrams*, 8th ed.; American Society for Metals: Metals Park, OH, 1973; Vol. 8.
34. March, J. *Advanced Organic Chemistry: Reactions, Mechanisms, and Structure*; Wiley: New York, 1992; pp 23−25.
35. Nessim, G. D.; Hart, A. J.; Kim, J. S.; Acquaviva, D.; Oh, J.; Morgan, C. D.; Seita, M.; Leib, J. S.; Thompson, C. V. Tuning of Vertically-Aligned Carbon Nanotube Diameter and Areal Density Through Catalysts Pre-Treatment. *Nano Lett.* **2008,** *8*, 3587–3593.
36. Chen, I.-C.; Chen, L.-H.; Orme, C.; Quist, A.; Lal, R.; Jin, S. Fabrication of High-Aspect-Ratio Carbon Nanocone Probes by Electron Beam Induced Deposition Patterning. *Nanotechnology* **2006,** *17*, 4322–4326.
37. Abramoff, M. D.; Magelhaes, P. J.; Ram, S. J. Image Processing with ImageJ. *Biophotonics Int.* **2004,** *11*, 36–42.